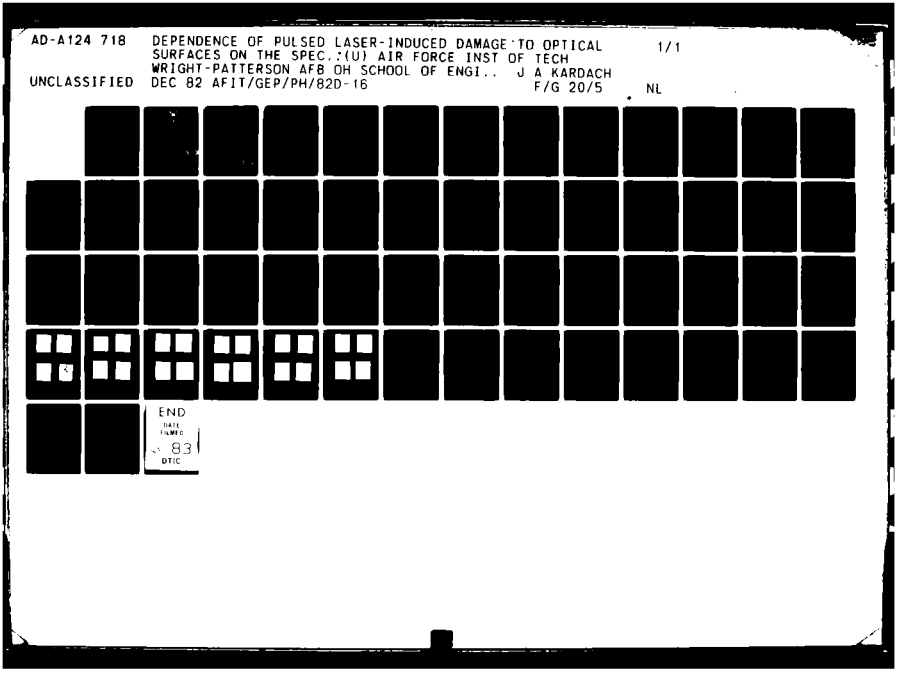
AD-A124 718
DEPENDENCE OF PULSED LASER-INDUCED DAMAGE TO OPTICAL SURFACES ON THE SPEC.:(U) AIR FORCE INST OF TECH WRIGHT-PATTERSON AFB OH SCHOOL OF ENGI.. J A KARDACH
1/1
UNCLASSIFIED
DEC 82 AFIT/GEP/PH/82D-16
F/G 20/5
NL
END
DATE FILMED
83
DTIC

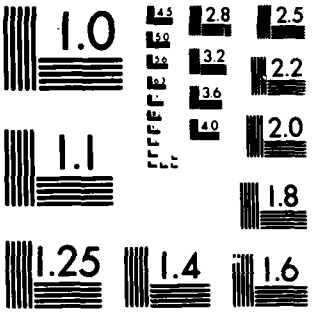

DEPARTMENT OF THE AIR FORCE
AIR UNIVERSITY (ATC)

AIR FORCE INSTITUTE OF TECHNOLOGY

Wright-Patterson Air Force Base, Ohio

Dependence of Pulsed Laser-Induced Damage to Optical Surfaces on the Species and Pressure of an Ambient Gas

Thesis

AFIT/GEP/PH/82D-16 John A. Kardach

AFIT/GEP/PH/82D-16

Dependence of Pulsed Laser-Induced Damage to Optical Surfaces on the Species and Pressures of an Ambient Gas

Thesis

Presented to the Faculty of the School of Engineering
of the Air Force Institute of Technology
Air University
in Partial Fulfillment of the
Requirements for the Degree of
Master of Science

by

John A. Kardach, B.S.
2nd Lt USAF
Graduate Engineering Physics

December 1982

Preface

This thesis covers a four month period of research carried out at the Air Force Weapons Laboratory (AFWL) at Kirtland AFB, New Mexico, and was supported by ILIR funds from AFWL. The project was to study the dependence of laser-induced damage to optical surfaces upon the pressure and species of the surrounding environment. If such a dependence upon the pressure and the type of environment exist, then there could possibly be space applications if the damage resistance or threshold of an optical surface is increased with the absence of an atmosphere. Also, if the damage resistance depends upon the type of environment, then one could increase the damage threshold by simply placing the material within an appropriate atmosphere.

This project was proposed by my advisor, Dr. Arthur H. Guenther, Chief Scientist of AFWL. Throughout the course of research, he provided much needed advice and encouragement.

I would like to also thank the many other people who gave their time and effort to help me with my research. My special thanks to Dr. Alan Stewart, for finishing the data on the leached ARG-2 Samples, and without whose help and encouragement in the lab, my progress would have been much more difficult. The visual examination of the many damage sites was performed by Mr. Ed Miesak, which allowed the large amounts of data to be obtained and analyzed. My thanks to Dr. C.J. Brinker and Mr. Mark Harrington of Sandia National Laboratories, Albuquerque, New Mexico, for supplying me with information on and a set of Sol-gel derived coatings. I wish to also thank Arthur Goodman for his excellent

photographic assistance, and Lt Col William F. Bailey for his comments and criticism on the writing of this thesis. Lastly, I would like to thank Trudy Landry for her understanding and moral support.

John A. Kardach

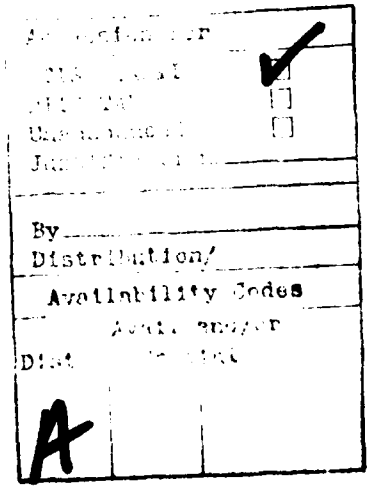

Contents

Page

Preface ii

List of Figures v

List of Tables vi

Abstract vii

I. Introduction 1

- Background 1
- Objectives 3
- Scope 4

II. Experiment 5

- Experimental Arrangement 5
- Experimental Components 7
- Optical Alignment 18
- Samples 20
- Damage Threshold Determination 22
- Accuracy of Results 25

III. Results and Conclusions 26

- Results 26
- Conclusions 27
- Comparison of Results 27
- Recommendations for Future Research 40

Bibliography 42

List of Figures

Figure		Page
1	Experimental Arrangement	6
2	Detail Schematic of the Laser System	8
3	Temporal Response of the Laser Pulse	10
4	Spatial Profile of the Laser Pulse	12
5	Two Wire Intensity Profiles for Three Different Positions About the Focal Region	13
6	The Sample Chamber	16
7	Laser Shot Pattern on Sample	18
8	Method for Determining the Energy Density Damage Threshold	24
9	Damage Morphology of ZrO_2 Thin Film Dielectric Coatings	32
10	Damage Morphology of Copper Mirror Samples	33
11	Damage Morphology of Unleached ARG-2	34
12	Damage Morphology of Bare Substrates of Fused Silica	35
13	Damage Morphology of Unleached Sol-Gel Derived Coatings	36
14	Damage Morphology of Leached Sol-Gel Derived Coatings	37

List of Tables

Table		Page
I	Damage Thresholds and Spreads for ZrO_2 and Copper Mirrors	28
II	Damage Thresholds and Spreads for Leached and Unleached ARG-2	29
III	Damage Thresholds and Spreads for Leached and Unleached Sol-Gel Derived Coatings	30
IV	Damage Thresholds and Spreads for Fused Silica Substrates	31

Abstract

The testing of optical materials in electronegative gases was investigated to determine if an increase in the resistance of the material to pulsed laser-induced damage could be realized as indicated by the Soviet literature.* The materials were irradiated with a 1.06 μm laser pulse of 5 nsec and a spot size ($1/e^2$ radius) of 148 μm. The materials used for testing consisted of ZrO_2 dielectric thin films ($\lambda/2$ at 1.06 μm), copper mirrors, fused silica substrates, Hoya's ARG-2 Glass, and porous sol-gel derived coatings. Each material was tested in environments of N_2, CF_4, and SF_6 for pressures ranging from less than 10^{-5} torr to 600 torr. The results indicated that the energy density damage threshold was unaffected by the type or pressure of the gas surrounding the material for single shot damage testing.

*Eron'ko, S.B., G.T. Petrovskii, A.V. Shatilov, A.K. Yakhkind, and L.V. Alcksandrova, "On Increasing the Resistance of Glass Surfaces to Repeated Radiation Loads", Sov. J. Opt. Technol., Vol 43, No. 1, pp. 29-31 (Jan 1976).

I. Introduction

Background

Laser-induced damage of optical train components critically limits the design and reliability of high power, high energy laser systems. The importance of this problem is such that an annual symposium, held since 1969 (Refs 1-12), has been devoted to the subject of laser-induced damage in optical materials.

The damage threshold, or the areal energy density at which damage occurs to a material, varies from material to material, and often depends upon the methods of fabricating and finishing the material (Ref 13) as well as upon the material's environment (Ref 14). For high powered and high energy laser applications, the laser beam must often be expanded to reduce the energy density of the beam below the damage threshold of the optical components. However, with an expanded beam, larger and heavier optical components are required. These larger optics are much more expensive and difficult to manufacture. Also, if there is a size and weight limitation on the laser system, then expanding the beam is not a viable approach. Thus, the study of laser-induced damage, and methods of increasing the resistance of materials to laser radiation becomes extremely important in the design of compact, light weight, high power, high energy laser systems.

The study of laser-induced damage has been going on since the beginning of the laser era, and there have been many theories proposed for predicting the process of laser breakdown and damage to the optical materials. Three of the most accepted theories on pulsed laser-induced breakdown are avalanche ionization, multiphoton ionization, and absorption by impurities.

Avalanche ionization (Refs 15–18) begins with electrons in the conduction band of a material interacting with the electric field of the laser radiation. The electric field accelerates an electron causing the electron to gain energy. As the electron is accelerated, it suffers collisions and loses energy. If the electron achieves enough energy before a collision, then it can impact ionize a valence electron. These two electrons then undergo the same energy gaining process to produce four free electrons through impact ionizations, and so on. This growth process continues until the number density of the electrons approaches 10^{18} cm^{-3}, where breakdown and a plasma occur. The plasma then more efficiently absorbs the laser radiation, and causes catastrophic and irreversible damage to the material through reradiation.

Multiphoton ionization (Refs 16,18,19,20) also concludes with the formation of a plasma and damage to the material, however, with the multiphoton process, the electrons gain energy through absorption of photons. In this process, the electrons are excited from the valence band to the conduction band during the first part of the laser pulse by direct absorption of two or more photons. The number of photons required for each ionization depends upon the band gap of the material and the wavelength of the laser. This exciting of electrons from the valence to conduction band in the multiphoton process is different from that of the avalanche process, which requires electrons to already be present within the conduction band in order for the process to proceed.

During the remaining portion of the laser pulse, the electrons acquire energy by an inverse bremsstrahlung process in which an electron acquires energy from a photon by absorption while in the presence of an atom or ion in order to conserve momentum. These electrons can then

impact ionize valence electrons, thus producing a rapid increase in the electron number density until breakdown and a plasma occur as in the avalanche ionization process.

Damage from absorbing impurities in the material (Refs 18,21,22,23) occurs through a thermal process. As an impurity absorbs enough energy, it can cause a localized melting or fracturing of the surrounding material. If the impurity lies at the surface of the material, then the heating results in an evaporation of the surrounding material and a plasma is formed. This plasma again absorbs the laser radiation and causes irreversible damage to the material.

Objectives

This research experimentally investigated the dependence of a material's damage threshold on the nature and pressure of selected ambient gases. Since laser damage to an optical surface generally proceeds through an electron avalanche process, the presence of a highly attaching gas species could possibly reduce the effective growth rate of the electron number density sufficiently to inhibit breakdown and damage during the laser pulse. A positive indication of this approach of increasing the resistance of materials to laser-induced damage is given by S.B. Eron'ko, G.T. Petrovskii, A.V. Shatilov, A.K. Yakhking, and L.V. Aleksandrova (Ref 24). Eron'ko, et. al found that filling a porous silica film with an electrically insulating filler (SF_6) lead to an increase in the damage resistance of that material. A more detailed comparison between Eron'ko's work and the work of this thesis will be discussed in a later section.

Scope

Between 8,000 to 12,000 laser test shots were analyzed during the course of the experiments. Six different types of samples were tested in three different gases for a variety of pressures ranging from less than 10^{-5} torr to 600 torr. The samples consisted of ZrO_2 dielectric thin films ($\lambda/2$ at 1.06μm), copper mirrors, fused silica substrates, Hoya's ARG-2 Glass, and porous sol-gel derived coatings. The gases used in the experiment were Nitrogen (N_2), Tetrafluoromethane (CF_4), and Sulfurhexafluoride (SF_6).

The selection of nitrogen served as a standard for testing and comparison purposes. CF_4 and SF_6 were selected because they are electronegative gases and will readily attach free electrons (Refs 25,26,27). In addition, CF_4 and SF_6 are fairly stable in the presence of an electrical discharge, and will not easily disassociate to produce corrosive by-products which could react with the samples or equipment (Ref 27).

II. Experiment

Experimental Arrangement

The experimental arrangement is shown in Figure 1. The arrangement was selected to split the laser beam into two equivalent paths; a high energy path for testing and a diagnostic path (Ref 28). The high energy path contained 99.9% of the beam energy and was used to perform the damage tests. The diagnostic path contained less than 0.1% of the beam energy and was used to determine the temporal and spatial profile of the laser beam at the damage site.

Since the diagnostic path was to characterize the beam at the damage site, it was crucial to have identical beam profiles for each path. To ensure identical beam profiles, the two lenses used in the experiment to focus the beam were chosen to have as nearly the same focal length (2m f.l.) as possible. Also, each lens was placed the same distance from the beam splitter. Since the beam exiting the laser was diverging, having the lenses the same distance from the beamsplitter ensured that the spot size of the beam incident onto each lens was the same.

The energy in the main beam path was varied with the use of a wave plate and a linear polarizer. Since the laser beam was linearly polarized, only a certain component of the beam's electric field would be transmitted by the polarizer,

$$E = E_o \cos \theta \quad , \tag{1}$$

where E_o is the incident electric field, and θ is the angle between the two axes of polarization. Thus, the irradiance of the beam leaving the

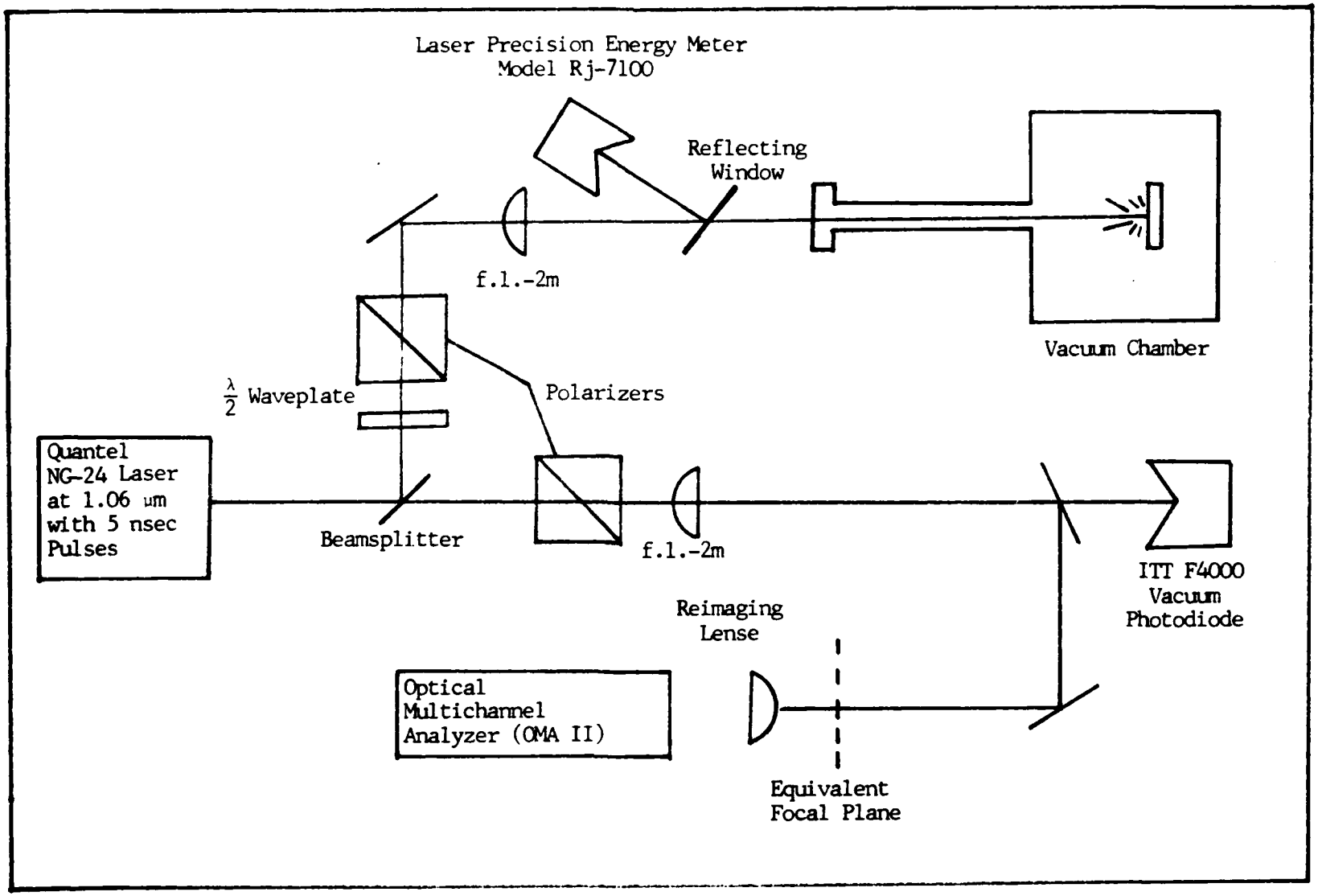

Figure 1: Experimental Arrangement

polarizer is

$$I = kE_o^2 \cos^2\theta \quad ,$$

where k is a constant. The wave plate was used to rotate the polarization of the laser beam, thus changing θ and controlling the irradiance of the beam as it leaves the polarizer.

The polarizer in the diagnostic path was to remove the various unpolarized components of the beam, and thus keep the spatial profile of the diagnostic beam consistent with that of the main beam path.

Experimental Components

The laser system* is shown in Figure 2. The laser system employs a Nd-YAG oscillator and pre-amplifier. The main amplifier of the system is a Nd^{3+} doped silicated glass rod. The laser was operated in the TEM_{oo} mode, and was Q-switched with a saturable dye *Bis* Dimethylamino (Benzil) nickel, (BDN), which was placed in the oscillator cavity at position 2. The pulse length of the laser was approximately 5 nsec (FWHM).

During the experiment, the laser was operated in two different modes: with and without the main amplifier in operation. Without the main amplifier in operation, the laser could damage all of the samples tested except for the bare substrates of fused silica and the unleached ARG-2 samples. With the amplifier in operation, all the samples could be damaged. However, with the main amplifier in operation, the laser

---

* Quantel Corporation, Model NG-24

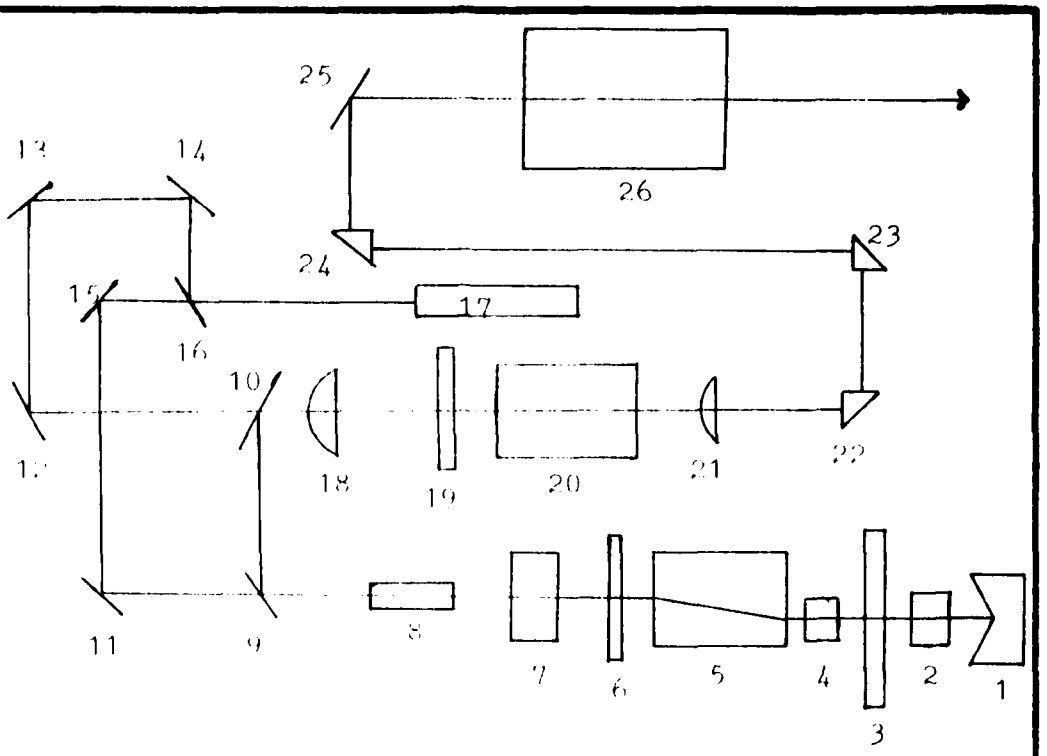

1. MS 390 with 5 mm RC mirror (R M 1.06 um)
2. BDN Saturable Dye
3. Beam Shutter
4. Polariser
5. HH 305 Laser Head
6. Spatial Filter
7. Output Mirror
8. Glass Etalon
9. Corner Mirror for 1.06 um
10. Corner Mirror for 1.06 um
11. Silver Mirror for HeNe
12. Silver Mirror for HeNe
13. Silver Mirror for HeNe
14. Silver Mirror for HeNe
15. Silver Mirror for HeNe
16. Beamsplitter
17. HeNe Laser
18. Lens
19. Spatial Filter
20. HH 304 Laser Head (Pre-Amplifier)
21. Lens
22. AR Coated 90° Prism
23. AR Coated 90° Prism
24. AR Coated 90° Prism
25. Corner Mirror for 1.06 um
26. CF 320-16 Laser Head (Main Amplifier)

Figure 2: Detail Schematic of the Laser System

could only be fired once every 90 seconds, compared to the laser firing rate of once every two seconds without the main amplifier in use. Thus, the main amplifier was brought into operation only to test the fused silica substrates and the unleached ARG-2 samples.

The temporal response of the laser pulse was recorded with a biplanar vacuum photodiode.* The rise time of the photodiode was measured at <0.5 nsec. The output signal of the detector was processed by a Transient Digitizer**, which is a high speed data acquisition instrument that digitizes the input analog signal. The digitized signal is displayed at a slower speed on a video monitor, and is transferred to a processor unit.*** The processor unit is programmed to calculate the full width at half the maximum intensity (FWHM) of each laser pulse. Figure 3 shows a computer output for a typical laser pulse.

The spatial profile of the laser beam was obtained with an optical multichannel analyzer**** (OMA). The OMA system consisted of a segmented silicon vidicon detector and a microprocessor.

The vidicon detector has an active area of 12.5 mm by 12.5 mm. This active area is composed of many small photodiodes, which are given a surface charge by a scanning electron beam. As photons strike the diodes, electron hole pairs are created which deplete the surface charge on the diodes. As the electron beam again scans the diodes, the current required to recharge each diode is measured. This current is then directly proportional to the laser energy incident onto the diode.

---

* ITT, Model F4000
** Tektronix, Model $7912
*** Tektronix, PDP-1134
**** Princeton Applied Research, OMA-II

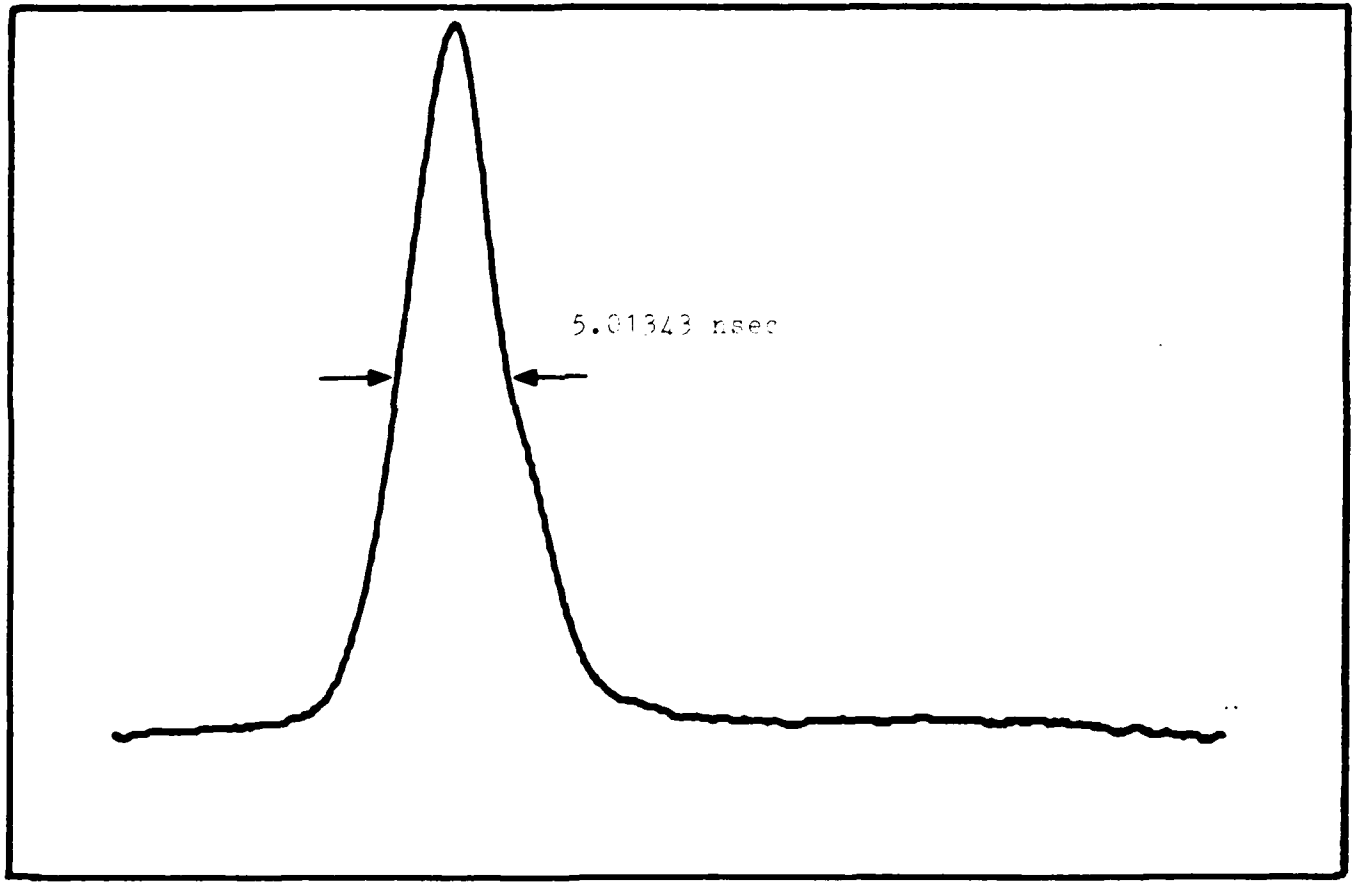

Figure 3: Temporal Response of the Laser Pulse (~5 nsec FWHM)

The vidicon was used to take a one-dimensional scan of the beam, and the intensity profile was stored on the microprocessor. Each scan contained 500 data points, with each data point representing the energy incident onto a slit 25 μm wide and 12.5 mm high. A beam profile taken by the OMA is shown in Figure 4.

Since the laser spot size ($1/e^2$ radius) is approximately 150 m, a beam scan taken by the OMA would only contain about six data points. Thus, to increase the resolution of the OMA, an imaging lens (7.5 cm f.l.) was used to slightly magnify the laser spot and image it into the vidicon detector.

The magnification of the imaging lens was determined with the use of two thin parallel wires. The two wires were frontly illuminated, and the reflected light was then imaged through the imaging lens into the vidicon detector. The separation of the two intensity peaks formed by the reflected light off of the wires was then determined. This separation was then compared to the actual separation of the two wires, and the magnification determined. The imaging lens was found to magnify the laser spot by 9.5X ± 5%.

The two wire method of determining the magnification was much more precise than trying to measure the thickness of a single wire. With a single wire, one has to define the "edge" of the wire on the intensity pattern, and also when the wire is in focus. Measuring the separation of the peaks from the two wire intensity profile is rather simple, and the separation of the peaks remains constant even if the wires are not exactly in focus, as shown in Figure 5.

A measurement of the beam's spatial profile on the OMA was to be taken with each damage shot. However, after the first couple of hundred

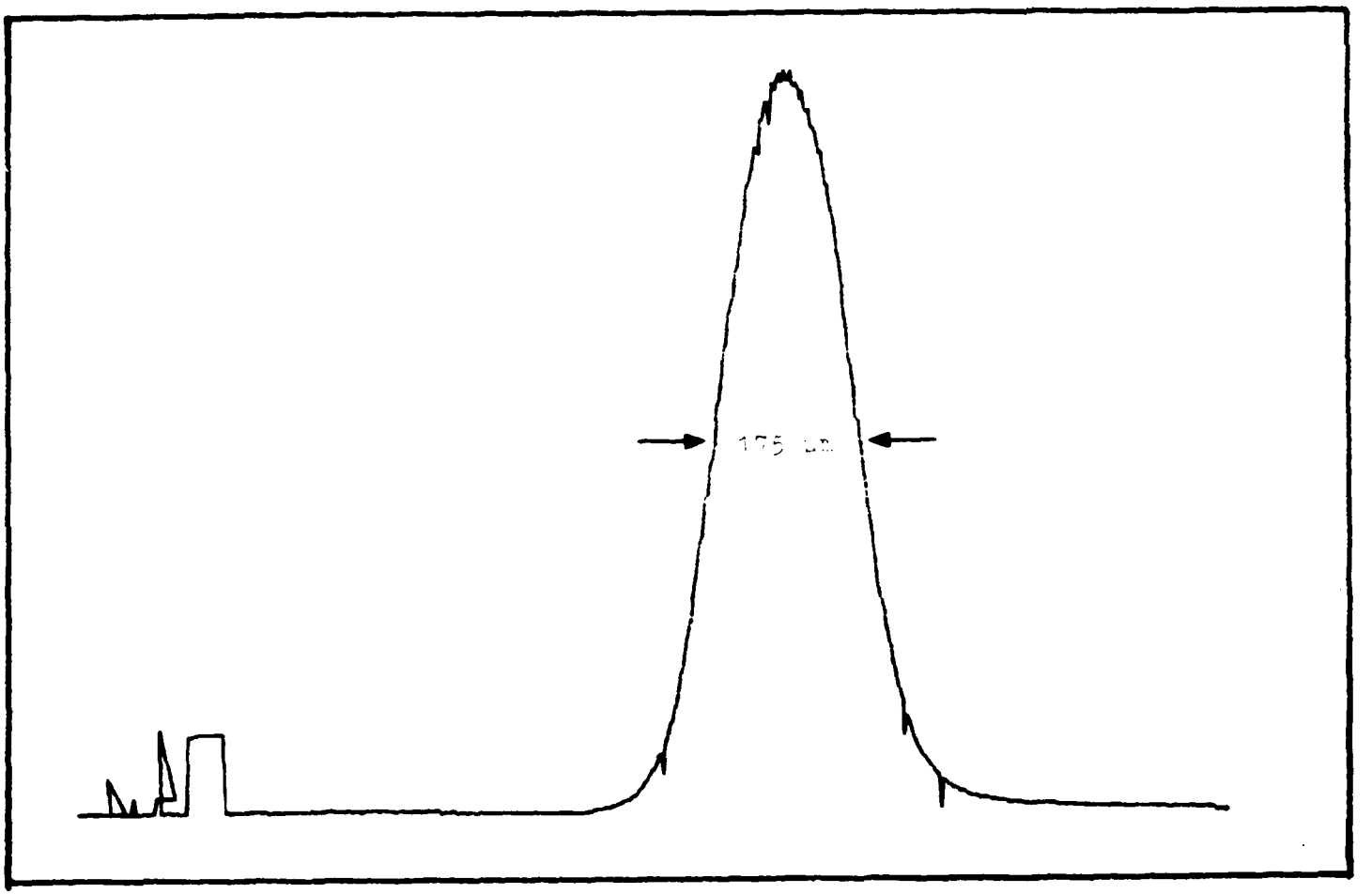

Figure 4: Spatial Profile of the Laser Pulse (FWHM = 175 µm)

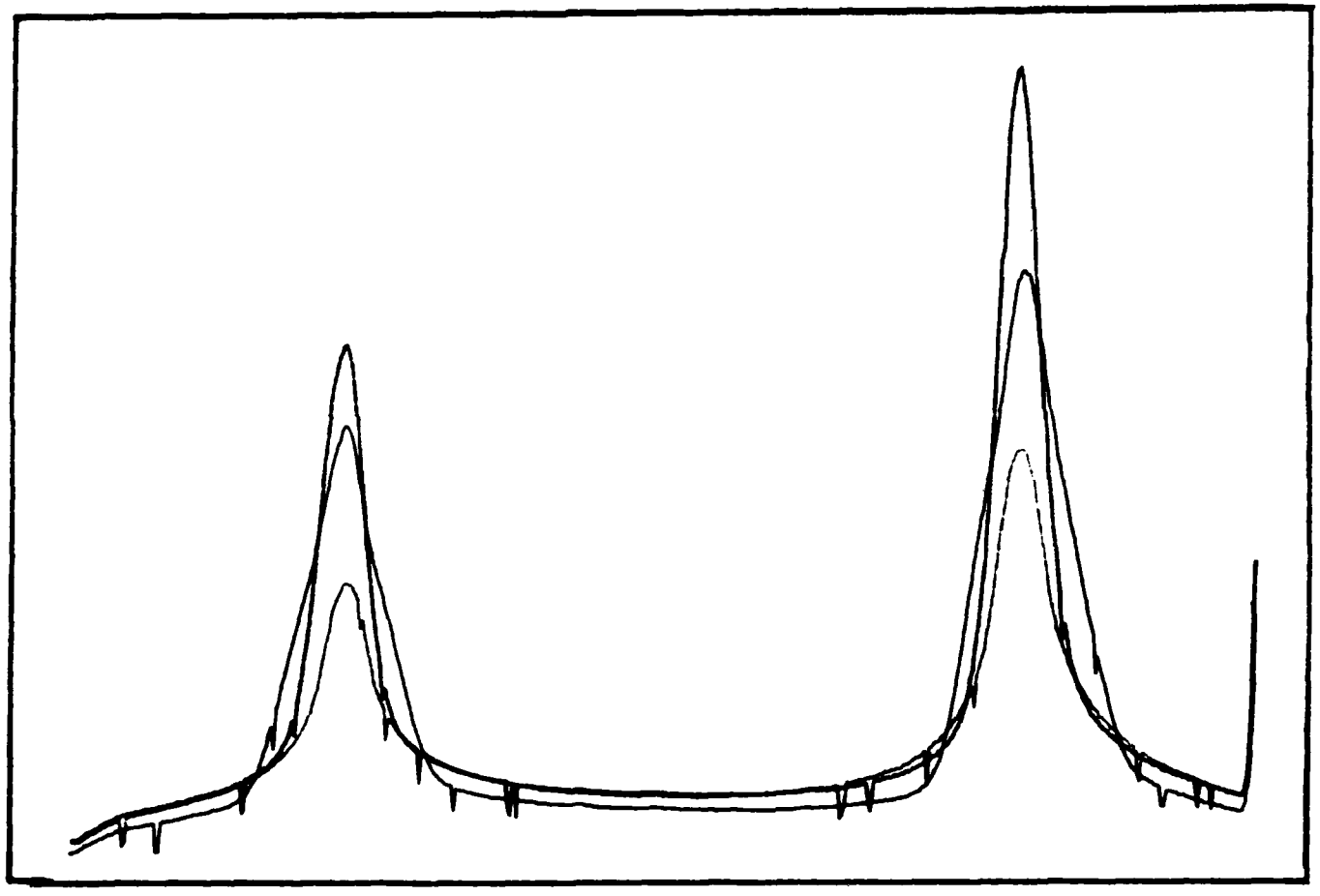

Figure 5: Two Wire Intensity Profiles for Three Different Positions About the Focal Region

shots, the beam profile remained constant with a 6% variation. Measurement of the profile was then limited to five shots at the beginning of each pressure run, and to five shots at the end of each run to check for variations in the profile.

The spot size of the beam was determined by measuring the FWHM of the profile obtained by the OMA. With the magnifying lens in place, a FWHM of 63 channels with a ±6% variation from shot to shot was obtained, which corresponds to a spot size ($1/e^2$ radius) of 148 μm with a variation of ±7.8%.

The energy of the main beam path was determined by measuring the energy reflected by a window placed in the beam path. The reflected energy was measured with a pyroelectric energy detector.* The detector has the following manufacturer's specifications:

Range:	1 μJ to 1 J
Maximum Peak Power:	1 MW/cm^2
Pulse Width:	< 1 nsec to 1 msec
Accuracy:	± 5% of Reading

The reflected energy measured represented a certain percentage of the energy striking the sample. The exact amount reflected was determined by measuring simultaneously the energy received at the sample site and the energy reflected from the window. For this measurement, another energy detector** was used to measure the energy received at the sample site. The detector has the following manufacturer's specifications:

Range:	2 μJ to 1 J
Maximum Energy Density:	1 J/cm^2

---

* Laser Precision, Model Rj-7100
** Laser Precision, Model Rk 3230 Pyroelectric Detector

Maximum Peak Power Density: 10^7 W/cm^2

Pulse Width: < 1 nsec to 1 msec

Accuracy: ± 4% of Reading (Detector fully Illuminated)

A number of the laser shots were measured over a wide range of energies, and the two detectors showed a linear response with a variation of ±1%. The amount of energy reflected by the window was determined to be 3.7% of the energy at the sample, with an uncertainty of ±7%.

The sample chamber is shown in Figure 6. The chamber was constructed of aluminum and could maintain pressures from less than 10^{-5} Torr to two atmospheres (1520 Torr).

The laser beam entered the chamber through a window which was extended 30 inches in front of the chamber by an aluminum tube. This extension prevented the window from becoming damaged during the experiment.

The gases to be used in the experiment, Nitrogen (N_2), Tetrafluoremethane (CF_4), and Sulfurhexafluoride (SF_6), were introduced into the chamber through a feedthrough valve after evacuation. During the experiment, each sample was first tested under vacuum conditions (10^{-5} Torr), and then tested at subsequent higher pressures (1 Torr, 50 Torr, 200 Torr, and 600 Torr). After a specific pressure was achieved, the sample chamber was allowed to equilibrate for an hour in order to allow the pressure to stabilize.

The vacuum system consisted of two vacuum pumps, a mechanical pump* and a cryopump.** The cryopump was run continuously and could be sealed off from the chamber with a butterfly valve when not needed. The

---

* Alcatel Mechanical Pump 2004A
** CTI-Cryogenics Cryo-Torr 7 High Vacuum Pump

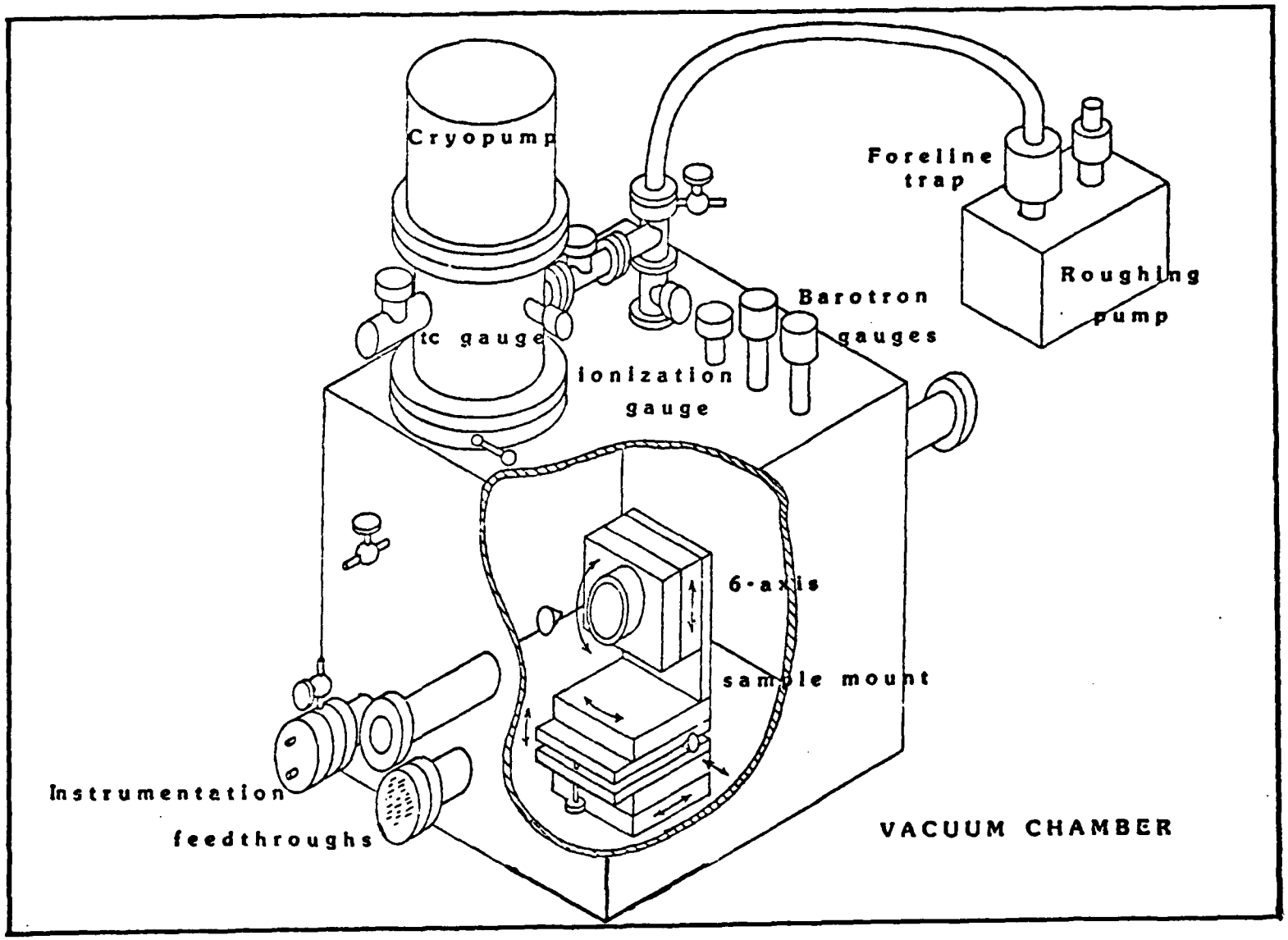

Figure 6: The Sample Chamber

mechanical pump was used to pump the chamber to less than 200 millitorr, and was then sealed off from the chamber. With the pressure less than 200 millitorr, the cryopump could be used by the opening of the butterfly valve. To achieve a base pressure of less than 10^{-5} Torr required a pumping time of about 90 minutes starting from room pressure. The pressure within the chamber was measured with three different pressure gauges; a baratron pressure gauge*, a thermo-couple gauge**, and an ionization gauge***. The baratron gauge had a range of 0.1 to 1000 Torr and was accurate to 0.5% of the pressure reading. The thermo-couple gauge had a range of 1 millitorr to 1 Torr, and the ionization gauge had a range of 1 millitorr to 10^{-8} Torr.

The sample holder was located in the center of the vacuum chamber. The holder had the capability to adjust the sample position along six different directions. The sample could be rotated around the beam's axis, tilted about two axes, or moved side to side, up and down, or forward and backward (see Figure 6). After the initial set-up of the experiment, only two of the directional capabilities, the rotation of the sample and the side to side movement of the sample, were used to orient the sample and present a new target site.

The target sites on the sample were situated in concentric circles about the center of the sample. The target sites making up each of the circles were spaced 1 mm apart, and the spacing between the concentric target rings was also 1 mm. However, the spacing for the fused silica and unleached ARG-2 samples was changed to 1.5 mm between target sites and

---

* MKS Baratron Gauge, Type 222AHS
** Veeco Thermocouple Gauge, Type DV-1M
***High Vacuum Products, Inc., G-75 Ionization Gauge

target rings due to the fact that high damage shots tended to overlap into the next target site. The shot pattern created on a sample is shown in Figure 7.

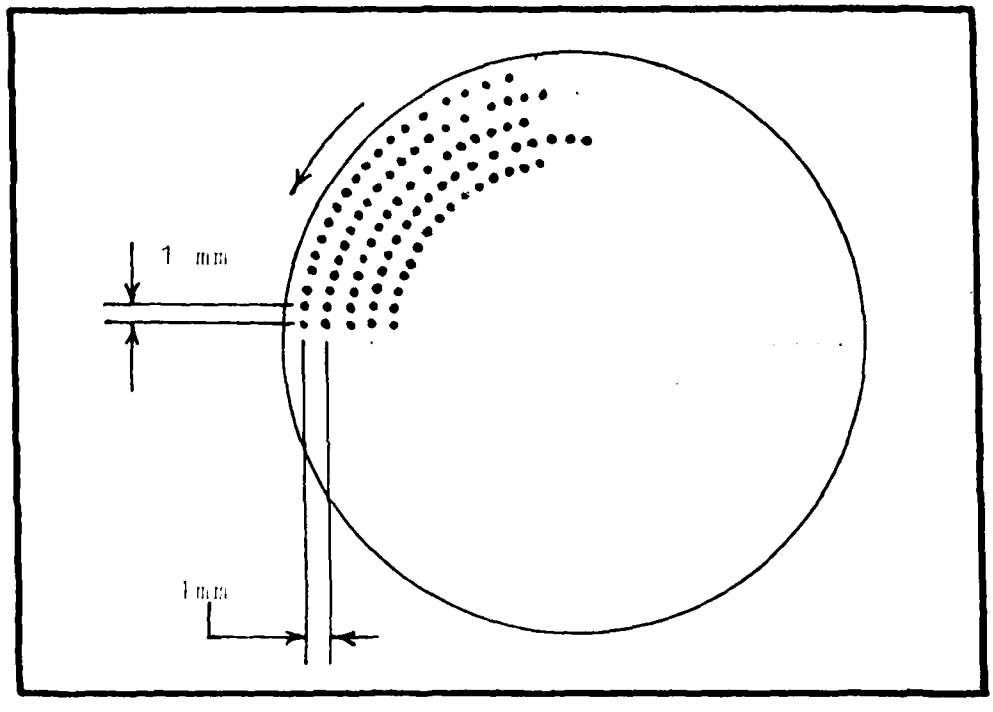

Figure 7: Laser Shot Pattern on the Sample

Each sample was observed during testing with the use of a prism and a telescope. The telescope had a 1.06 μm blocking filter placed before it, and the observer always wore safety goggles when viewing the sample during testing. The viewing of the sample during the laser shots was to observe whether or not a visible plasma was formed.

Optical Alignment

The optical alignment of the system was important, particularly as the diagnostic path was to duplicate the main path (Ref 28). First, as each

optical component was placed in the beam, it was centered such that the beam was incident onto the center of the component. Next, the lens in the main beam path was adjusted until the beam was focused at the sample site. The focal region of the lens was determined by taking beam scans at the sample site to determine the beam profile or spot size. The beam was focused at the sample site, when the beam scan at the sample provided the smallest beam profile.

The focusing lens in the diagnostic path was then positioned the same distance from the beamsplitter as the lens in the main beam path. Next, the distance between the vidicon detector and the imaging lens was adjusted to provide the magnification required for proper resolution, and then the distance was fixed by the use of metal spacers placed between the vidicon and the imaging lens. The imaging assembly (the vidicon detector and the imaging lens) was then moved into focus by determining the position of the smallest beam profile with the use of the OMA.

Next, a sample was placed into the sample holder, and the holder was adjusted until the reflected beam made a 2^{o} angle with the incident beam. This angle prevented the reflected beam from feeding back into the laser system.

Each sample was etched with a diamond scribe on the edge to serve as a reference mark for placement into the sample holder. This reference mark allowed the sample to be removed from the holder, examined for damage under the microscope, and then replaced into the holder to be damaged again without the fear of losing one's orientation of the sample sites.

Each ring of sample sites was started along the same radial, and then the sample was rotated counterclockwise after each shot. After a ring was finished, the sample was rotated clockwise back to the first

sample site and then repositioned to a new target radius. The damage testing was begun upon the innermost ring, of each sample then moved to the next outer ring, and so on out to the edge of the sample. The innermost target ring primarily had a radius of 4 mm, but the ZrO_2 and fused silica samples contained a molybdenum disc in the center of the sample; for these samples, the innermost target ring began upon the 9 mm radius.

Samples

The samples used in this experiment consisted of Zirconium Oxide (ZrO_2) dielectric thin film coatings($\lambda/2$ at 1.06 μm), diamond turned copper, bare substrates of fused silica (SiO_2), leached and unleached Hoya's ARG-2 Glass, and leached and unleached Sol-Gel derived coatings on fused silica substrates. All the samples, except for the Sol-Gel samples, were made to Bennett size specifications, 1.52" +.005", -.000" in diameter and ~3/8" thick. The Sol-Gel samples were ~1.5" in diameter and ~1/4" thick.

The ARG-2 samples were produced by Hoya Optic U.S.A., Inc. The ARG-2 samples are made from a phase separable glass which, when chemically leached, produces a graded refractive index layer. This graded index layer is produced by micropores introduced by the leaching process, and this layer acts as an anti-reflection coating (Ref 29).

The Sol-Gel samples were produced by C. J. Brinker, Sandia National Laboratories, Albuquerque, New Mexico. According to Brinker et. al. (Refs 30,31,32), in the Sol-Gel process, glass-like macromolecules are formed in solution at room temperature by chemical polymerization. This polymerization process normally proceeds until the solution transforms to a stiff, amorphous, transparent gel. However, before the solution

transforms into a gel, it can be diluted in alcohol and then applied to a surface by spraying, dipping, or other thin film coating techniques. After drying, the surface is heated to remove residual organic matter, leaving an oxide layer. This layer is microporous and can be converted to an anti-reflection film by chemical etching.

The Sol-Gel samples used were coated with multicomponent silica gels of composition $66SiO_2 - 18B_2O_3 - Al_2O_3 - 6Na_2O - 3BaO$, on fused silica bare substrates. All samples contained five coats applied by spin coating at 2500 rpm. The coatings were heated at 500° C for 1000 minutes, and the leached samples were etched for 10 seconds in diluted acid, H_2SiF_6. The Sol-Gel coatings had a projected surface area of $10m^2/\mu m$, and the micropores were between 10 - 20 Å in size for the unleached samples and 30 - 40 Å for the leached samples. The thickness of the coatings were ~3500 Å.

In examining the Sol-Gel coatings, it was found that the coating thicknesses were slightly non-uniform and that there were slightly more defects in the Sol-Gel coating than in a normal dielectric coating. Also, the coatings were somewhat fragile and were easily scratched.

Each sample was cleaned prior to being placed into the vacuum chamber. First, each sample was blown free of dust by a filtered air can. Next, an alcohol wipe was performed. A 3 x 5 inch sheet of lens cleaning paper was placed upon the top of the sample, and then a drop or two of spectral grade ethanol was placed onto the tissue, wetting the sample underneath. The lens paper was then pulled across the sample and the surface allowed to dry. This procedure was repeated for all of the samples except the Sol-Gel and the leached ARG-2 samples which were only blown free of dust.

Damage Threshold Determination

The ideal situation for threshold determination would be to examine each target site for damage immediately after the laser shot. If laser damage did occur, then the next laser shot would be at a lower energy in order to determine the energy where damage will not occur. If damage does not occur, then the next shot would be at a higher energy in order to determine the energy where damage will occur. In this way, one could easily bracket the damage threshold of a sample. However, with the sample enclosed within the vacuum chamber, examination of the sample after each laser shot was not practical.

To determine the damage threshold of a sample, two separate series of shots were taken. The first series of shots was a set of 30 to 40 ranging shots. These ranging shots were taken at each separate pressure for each sample. The sample was then removed from the chamber and examined for damage under the microscope. Since these ranging shots covered a wide range of energies, from very low energies to energies where a visible plasma or spark could easily be seen, a rough estimate of the damage threshold could be made. The sample was then replaced within the chamber, and the remaining target sites were shot within this estimated damage threshold region.

This estimated damage threshold region was usually taken to be between the highest energy at which damage did not occur plus about 50% of that energy, and the lowest energy at which damage did occur minus about 50% of that energy. The total number of damage shots per pressure depended upon the sample, but was between 120 and 160 shots.

Laser damage to the sample was determined by a visual observation

of the damage sites under a Nomarski microscope. An observance of a visible plasma was taken as a sign of damage, but was not used as an indicator. Since the back surfaces often damages before the front surface (Ref 34), a visible plasma could mean damage to the back surface but not necessarily the front. In fact, a visible plasma was often observed for many damage shots, but no damage was observed under the microscope for these sites.

The magnification used for observing damage to the sample varied depending upon the damage site, but was between 100X and 500X. The sample was considered to be damaged if there was any observable change to the surface of the sample such as pits, halo formation, annealing, etc.

For ease in the location of the target sites with the microscope, highly damaging laser shots were made as markers on the sample. Each target ring was begun with two marker shots, and every third shot thereafter was a marker shot.

A complete shot record was kept on each sample used. The data recorded consisted of the laser pulse length, the energy of the laser shot, and the target site's radius and position. With the use of this shot record and the marker shots on the sample, one could easily locate any desired target site under the microscope. This technique was used to obtain the photographs of damage sites appearing within this thesis.

Figure 8 shows a typical data plot using the procedures of Bettis, House, and Walker (Refs 28,35,36). The damage threshold was determined by

$$E_{th} = (E_{ND} + E_{D})/2 \qquad (3)$$

where E_{th} is threshold energy density, E_{ND} is the highest energy density,

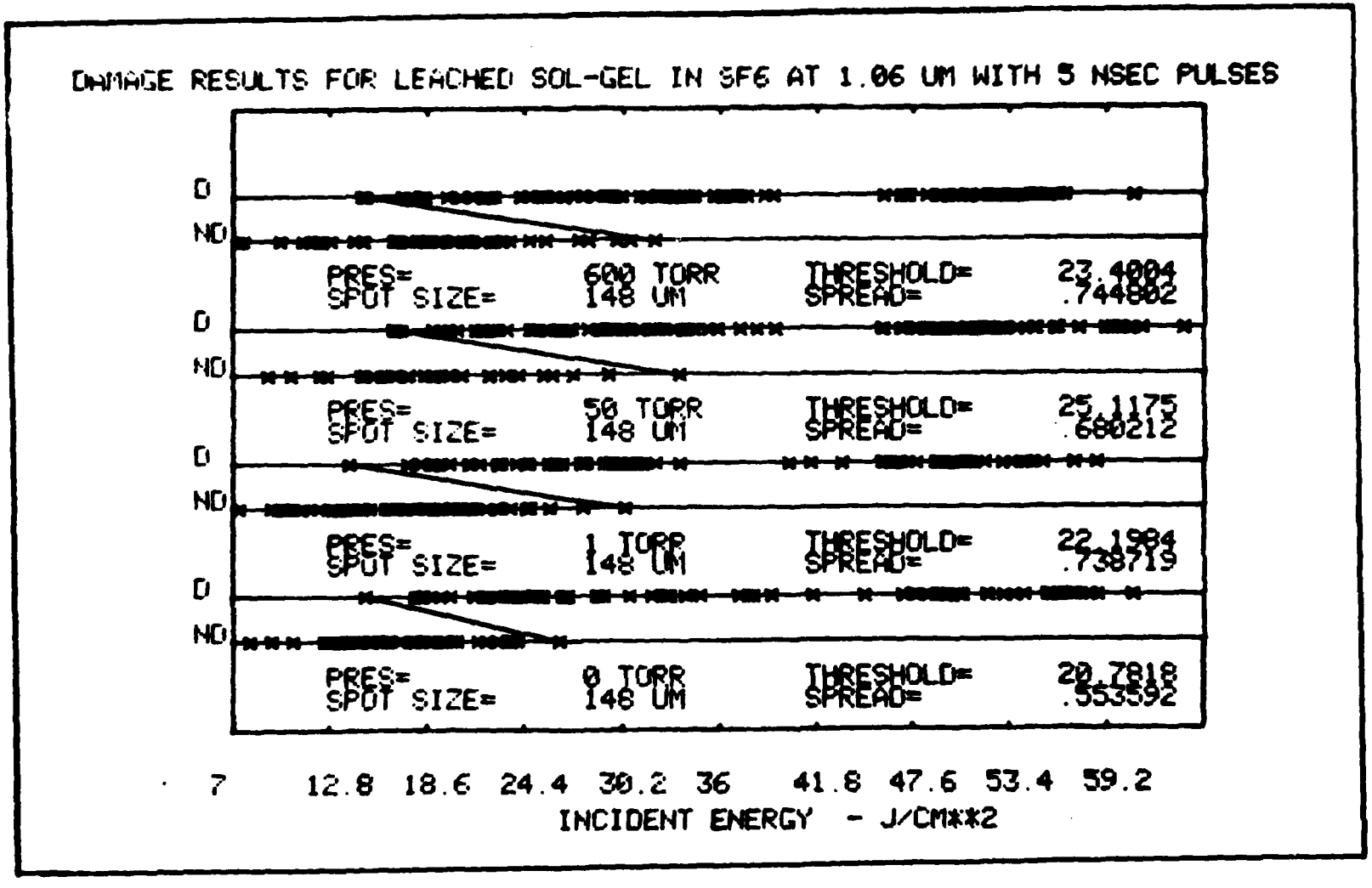

Figure 8: Method for Determining the Energy Density Damage Threshold

D = Damage, ND = No Damage

E_{ND} is the highest energy density at which no damage occured, and E_D is the lowest energy density at which damage occurred. The spread in the damage threshold, E_s, which is usually taken as a measure of the statistical nature of the damage process, is given by

$$E_s = \frac{2(E_{ND} - E_D)}{(E_{ND} + E_D)} \tag{4}$$

The spread actually gives an indication of how accurate or precise the damage threshold value is. Since there is an overlap region of energy densities at which both damage and no damage occur, as seen in Figure 8, the value for the damage threshold can actually be anywhere within this region. The damage criteria used for this experiment takes the threshold as the center value of this region. However, a spread is also given along with the threshold value which yields information about this overlap region. A large spread means that the overlap region is also large, and the value given for the threshold may be a somewhat inaccurate estimate. However, a small spread means that the overlap region is also small and that the value given for the threshold is a good estimate.

Accuracy of Results

The measured FWHM on the OMA has a variation of ±6% from shot to shot, and, including the uncertainty of the magnification of ±5%, this combination yields an uncertainty in the spot size measurement of ±7.8%. The measured energy has an uncertainty of ±8.6% due to the ±5% uncertainty of the Rj-7100 pyroelectric detector and the ±7% uncertainty in the amount of energy reflected by the window. Thus, with a ±7.8% uncertainty in the spot size measurement and ±8.6% uncertainty in the measured energy, a ±17.8% uncertainty is calculated for the measured energy densities.

III. Results and Conclusions

Results

Each sample was tested in three different gases, Nitrogen (N_2), Tetrafluoromethane (CF_4), and Sulfurhexafluoride (SF_6), except for the fused silica substrates and the unleached ARG-2 samples which were only tested in N_2 and SF_6. Each sample was tested for pressures ranging from a vacuum of less than 10^{-5} torr to 600 torr.

The testing of a specific gas at the various pressures on a certain type of sample were all performed upon the same sample. Thus, for example, only one copper mirror sample was tested in nitrogen for pressures of a vacuum, 1, 50, 200, and 600 torr. This precaution of using the same sample for the testing of a gas at the various pressures was to insure that the data taken for a certain type of sample in a specific gas was consistent from pressure to pressure.

A problem often encountered when comparing the damage thresholds of similar samples is that the threshold values can often disagree. The fabrication techniques, the handling of the sample, and many other factors can all affect the damage threshold of a sample. Even samples which are supposed to be identical in fabrication and preparation can give different values for the damage threshold of the material.

An example of this variation of damage thresholds from sample to sample is shown in Table II for the unleached ARG-2 samples. Comparing each ARG-2 sample under vacuum conditions, one sees that one sample has a much higher threshold (74.5 J/cm^2) than the other two samples (56.0 J/cm^2 and 58.4 J/cm^2).

The measured energy densities of the damage thresholds for the samples

tested are presented in Tables I to IV. The spread of the thresholds, given in parenthesis below the energy densities, represent a measure of the statistical nature of the damage process and are determined by equation (4).

Figures 9 to 14 show typical damage morphology for each of the samples tested. As the figures show, damage to the various materials ranged from minor damage of small pits, to massive damage of the sample.

Conclusions

The results indicate no real dependence of the energy density damage threshold upon the type or the pressure of a surrounding gas for any of the samples tested. However, if a small trend were present within the data, it could well be hidden within the wide spreads of the damage threshold measurements.

The results do indicate that the damaging process does not begin within the air near the surface of the sample. If the damaging process began within the air near the surface, then there would be a change of the damage threshold from vacuum conditions to higher pressures, since there is a pressure dependence in gas breakdown. However, the damage thresholds measured for the samples tested remained basically constant from pressure to pressure. This result supports findings by C. Yamanaka, et. al. (Ref 13), where the results of spectroscopic measurements of glass surface breakdown indicated only spectrum typical of the glass, and not that of the surrounding atmosphere.

Comparison of Results

In comparing the results of this research with that of S. B. Eron'ko,

DAMAGE THRESHOLDS AND SPREADS

SAMPLE	GAS	VACUUM ($<1\times10^{-5}$ TORR)	PRESSURES 1 TORR	60 TORR	200 TORR	600 TORR
ZrO_2	N_2	9.9 J/cm^2 (0.513)	10.7 J/cm^2 (0.[illegible])	9.6 J/cm^2 (0.633)	10.7 J/cm^2 (0.412)	9.2 J/cm^2 (0.669)
	CF_4	11.2 J/cm^2 (0.5[illegible])	12.6 J/cm^2 (0.628)	13.9 J/cm^2 (0.414)	12.9 J/cm^2 (0.293)	[illegible] J/cm^2 (0.474)
	SF_6	11.8 J/cm^2 (0.546)	10.0 J/cm^2 (0.611)	10.9 J/cm^2 (0.608)	11.4 J/cm^2 (0.560)	[illegible] J/cm^2 (0.474)
Cu Mirrors	N_2	3.4 J/cm^2 (0.639)	3.5 J/cm^2 (0.554)	4.0 J/cm^2 (0.614)	3.9 J/cm^2 (0.589)	3.7 J/cm^2 (0.647)
	CF_4	3.2 J/cm^2 (0.469)	3.4 J/cm^2 (0.730)	3.5 J/cm^2 (0.933)	4.0 J/cm^2 (0.589)	3.7 J/cm^2 (0.647)
	SF_6	2.4 J/cm^2 (0.818)	2.4 J/cm^2 (0.998)	2.1 J/cm^2 (0.794)	2.6 J/cm^2 (0.823)	2.4 J/cm^2 (0.955)

Table I: Damage Thresholds and Spreads for ZrO_2 and Copper mirrors - (Spreads are given in parenthesis)

DAMAGE THRESHOLDS AND SPREADS

SAMPLES	GAS	PRESSURES VACUUM ($<10^{-2}$ TORR)	50 TORR	600 TORR
UNLEACHED ARG-2	N_2	74.5 J/cm^2 (0.566)	81.7 J/cm^2 (0.504)	76.0 J/cm^2 (0.665)
	CF_4	56.0 J/cm^2 (0.939)	48.9 J/cm^2 (0.646)	62.5 J/cm^2 (1.005)
	SF_6	58.4 J/cm^2 (0.369)	54.7 J/cm^2 (0.341)	69.6 J/cm^2 (0.976)
LEACHED ARG-2	N_2	38.0 J/cm^2 (1.446)	39.8 J/cm^2 (1.426)	50.3 J/cm^2 (1.508)
	SF_6	21.2 J/cm^2 (1.143)	25.7 J/cm^2 (0.661)	23.8 J/cm^2 (1.454)

Table II: Damage Thresholds and Spreads for Leached and Unleached ARG-2 - (Spreads are given in parenthesis)

DAMAGE THRESHOLDS AND SPREADS

			PRESSURED		
SAMPLE	GAS	VACUUM (1 x 10^{-6} TORR)	1 TORR	50 TORR	600 TORR
UNLEACHED SOL-GEL DERIVED COATINGS	N_2	14.9 J/cm^2 (0.433)	20.5 J/cm^2 (0.357)	22.2 J/cm^2 (0.573)	25.0 J/cm^2 (0.437)
	CF_4	23.5 J/cm^2 (0.531)	20.5 J/cm^2 (0.269)	20.6 J/cm^2 (0.325)	15.7 J/cm^2 (0.630)
	SF_6	23.5 J/cm^2 (0.552)	21.6 J/cm^2 (0.614)	21.6 J/cm^2 (0.518)	18.3 J/cm^2 (0.801)
LEACHED SOL-GEL DERIVED COATINGS	N_2	18.7 J/cm^2 (0.722)	19.6 J/cm^2 (0.526)	23.8 J/cm^2 (0.443)	18.4 J/cm^2 (0.187)
	CF_4	21.6 J/cm^2 (0.545)	25.7 J/cm^2 (0.711)	26.0 J/cm^2 (0.508)	
	SF_6	20.8 J/cm^2 (0.554)	22.2 J/cm^2 (0.739)	25.1 J/cm^2 (0.680)	23.4 J/cm^2 (0.745)

Table III: Damage Thresholds and Spreads for Leached and Unleached Sol-Gel Derived Coatings - (Spreads are given in parenthesis)

SAMPLE	GAS	DAMAGE THRESHOLDS AND SPREADS AT VARIOUS PRESSURES		
		VACUUM (<10^{-5} TORR)	50 TORR	600 TORR
FUSED SILICA SUBSTRATE (SiO_2)	N_2	73.7 J/cm^2 (0.665)	63.1 J/cm^2 (0.430)	60.0 J/cm^2 (1.170)
	SF_6	77.2 J/cm^2 (0.532)	61.4 J/cm^2 (0.527)	74.7 J/cm^2 (0.972)

Table IV: Damage Thresholds and Spreads for Fused Silica Substrates - (Spreads are given in parenthesis)

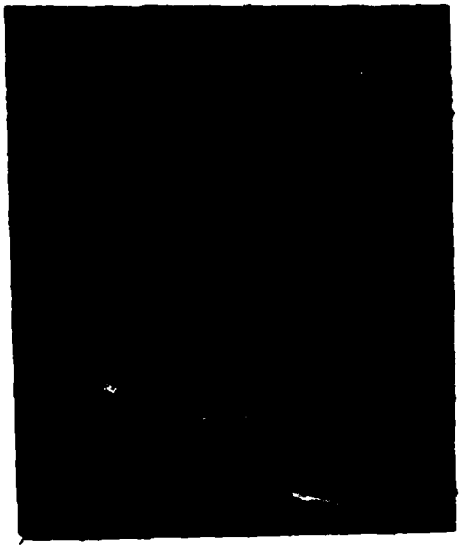

a. N_2 at Vac
Mag = 250X

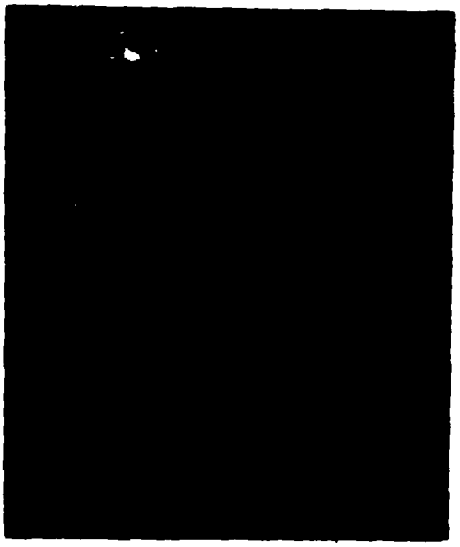

b. CF_4 at Vac
Mag = 250X

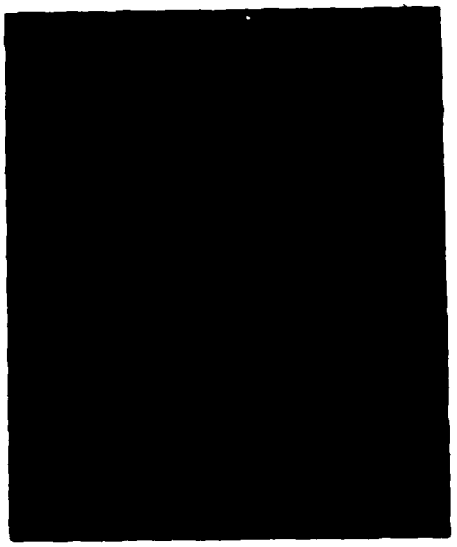

c. CF_4 at 200 Torr
Mag = 250X

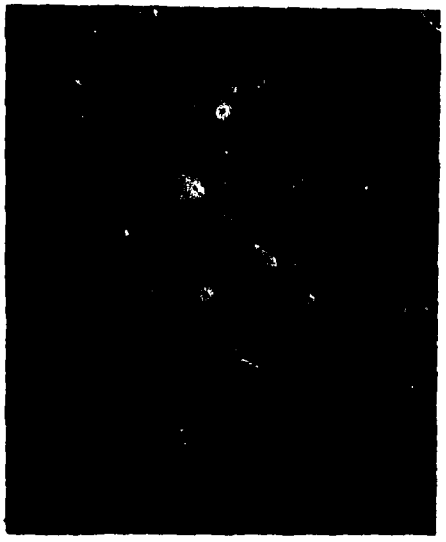

d. SF_6 at 200 Torr
Mag = 250X

Figure 9: Damage Morphology of ZrO_2 Thin Film Dielectric Coatings[2] ($\lambda/2$ at 1.06 μm)

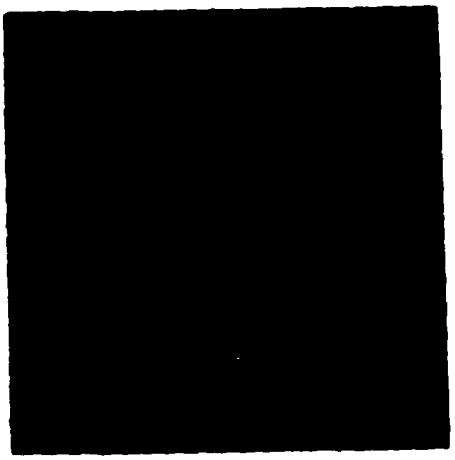

a. N_2 at 200 torr
Mag = 250X

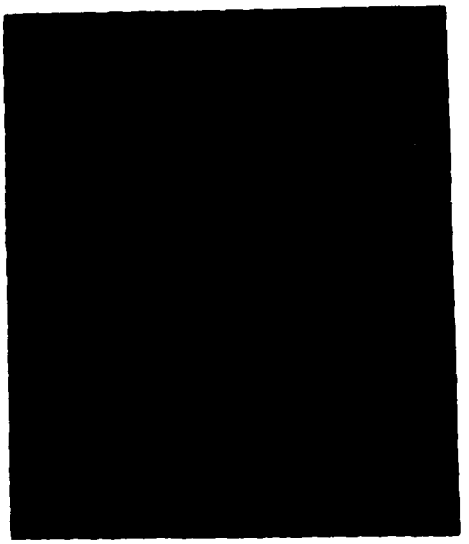

b. CF_4 at 50 torr
Mag = 500X

c. CF_4 at 1 torr
Mag = 250X

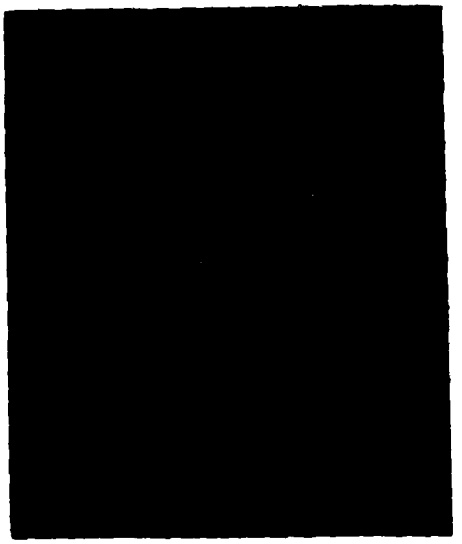

d. SF_6 at 600 torr
Mag = 250X

Figure 10: Damage Morphology of Copper Mirror Samples

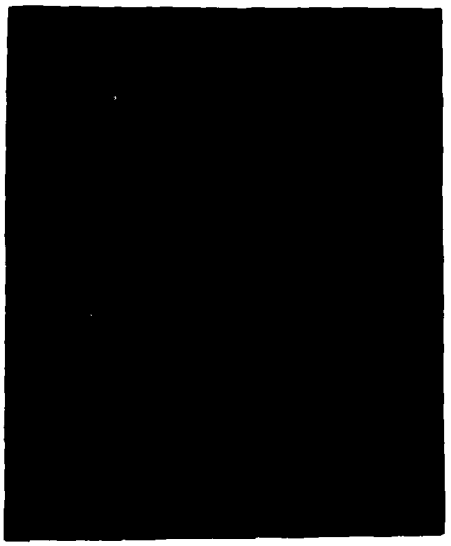

a. N_2 at Vac
Mag = 200X

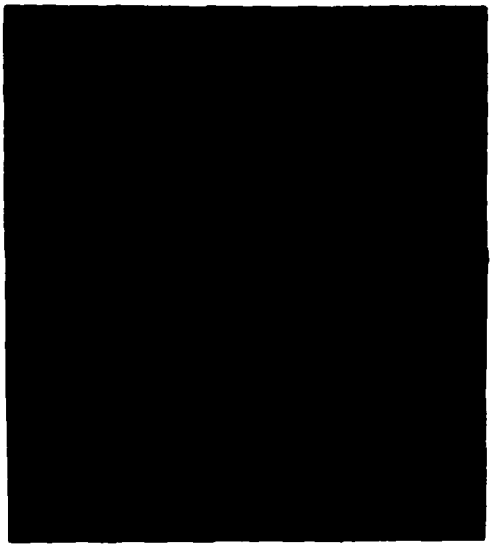

b. CF_4 at 600 torr
Mag = 100X

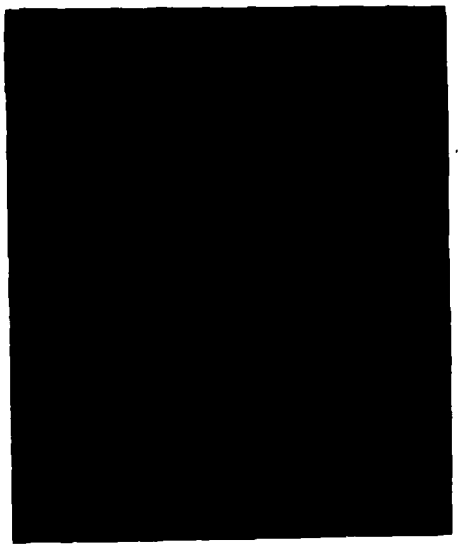

c. CF_4 at 50 torr
Mag = 100X

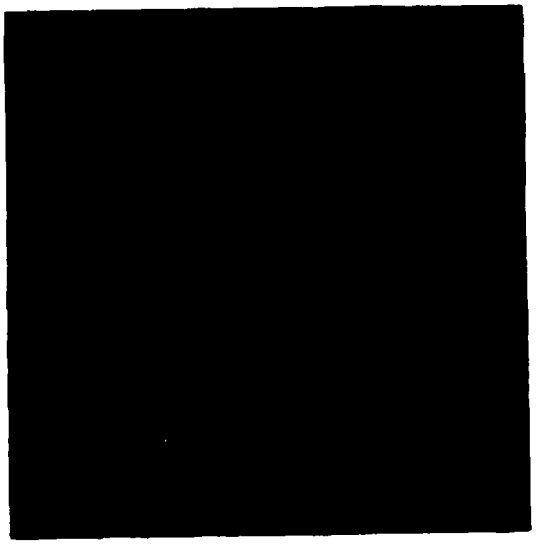

d. SF_6 at 50 torr
Mag = 50X

Figure 11: Damage Morphology of Unleached ARG-2

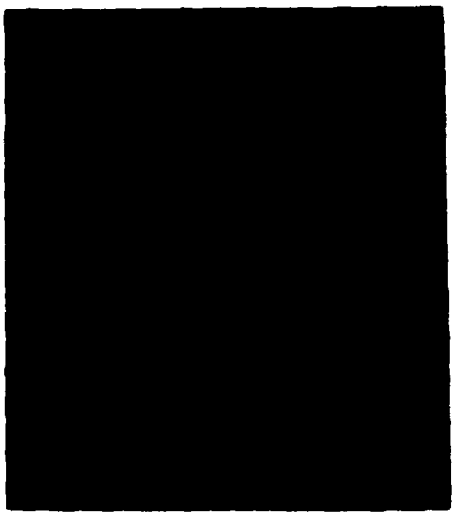

a. N_2 at 50 torr
Mag = 100X

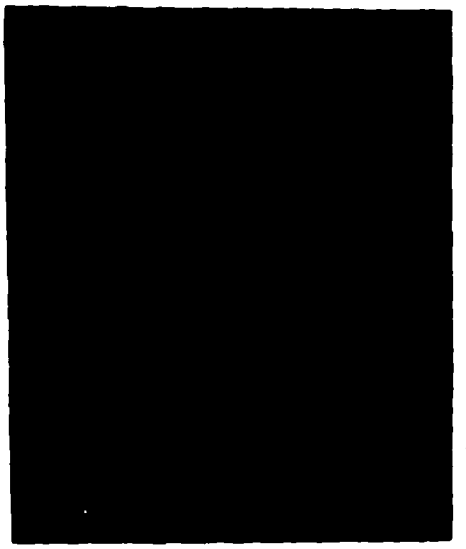

b. N_2 at 600 torr
Mag = 100X

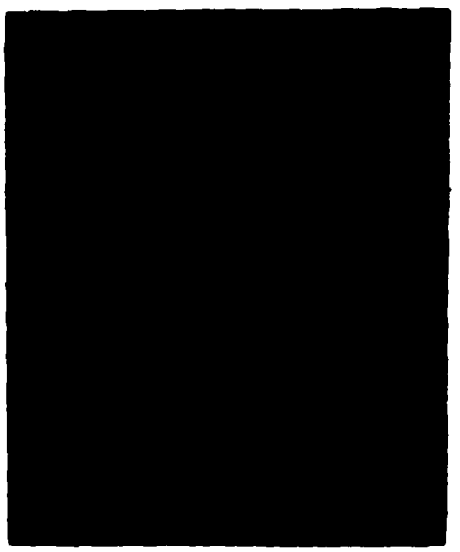

c. SF_6 at Vac
Mag = 100X

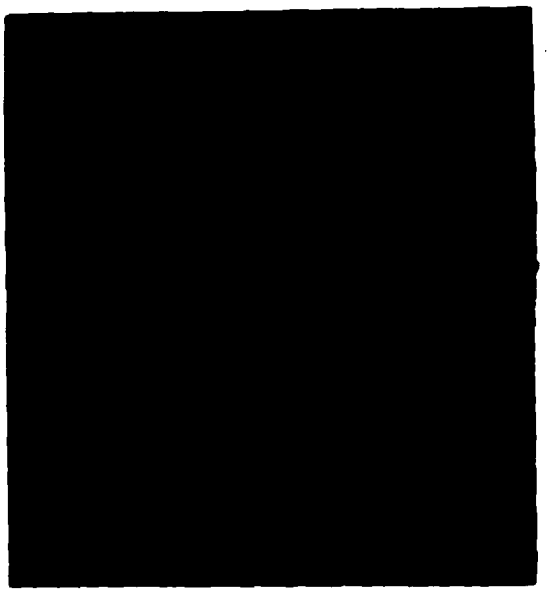

d. SF_6 at 600 torr
Mag = 100X

Figure 12: Damage Morphology of Bare Substrates of Fused Silicate

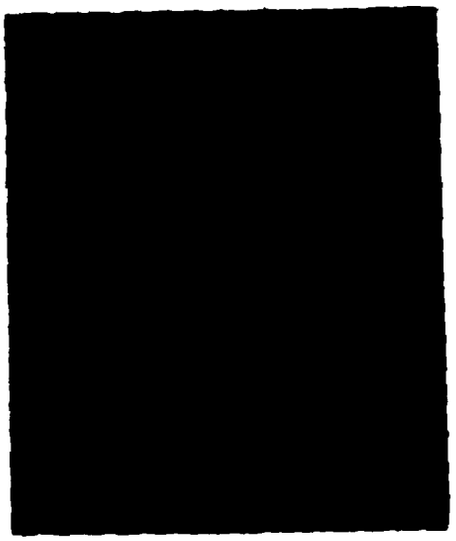

a. N_2 at Vac
Mag = 100X

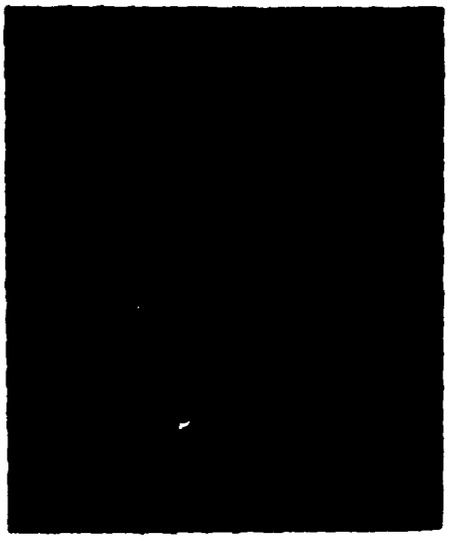

b. N_2 at 600 torr
Mag = 100X

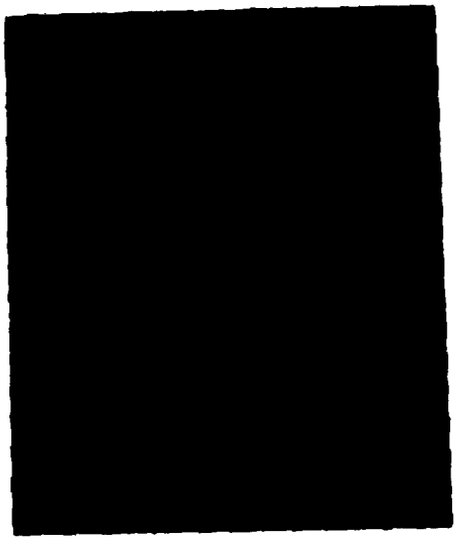

c. CF_4 at 600 torr
Mag = 100X

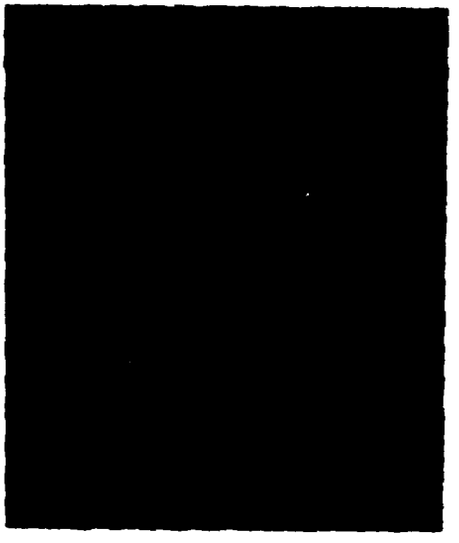

d. SF_6 at Vac
Mag = 100X

Figure 13: Damage Morphology of Unleached Sol-Gel Derived Coatings

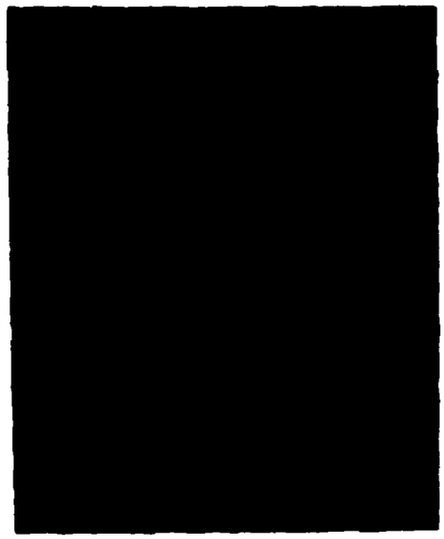

a. N_2 at 1 torr
Mag = 100X

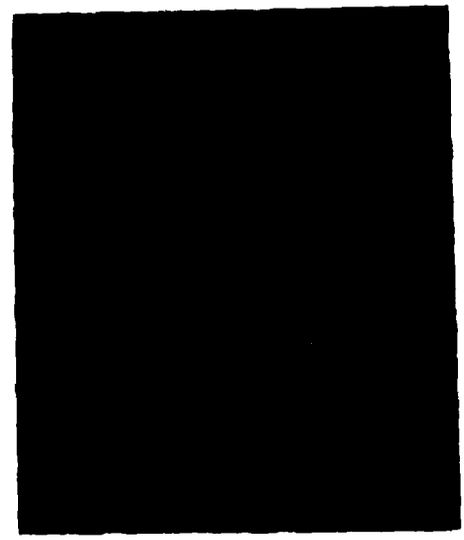

b. N_2 at 50 torr
Mag = 100X

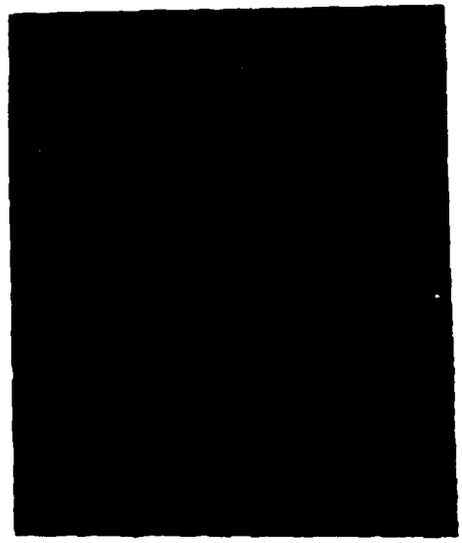

b. CF_4 at 1 torr
Mag = 100X

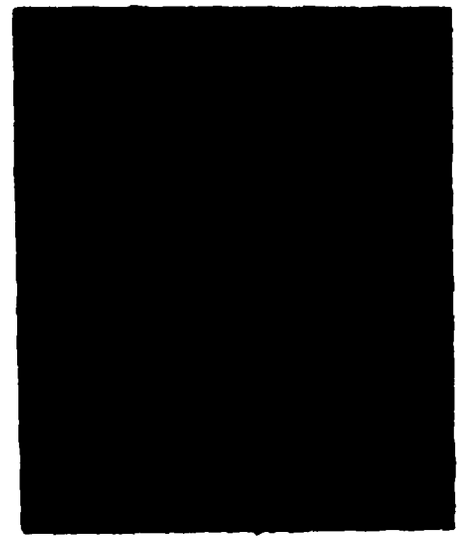

d. SF_6 at 1 torr
Mag = 100X

Figure 14: Damage Morphology of Leached Sol-Gel Derived Coatings

et. al. (Ref 24), one finds that the results are contradictory. Eron'ko, et. al., found that filling a porous silica film with an electrically insulating filler (SF_6) leads to an increase in the damage resistance of that material. However, results from this experiment, that of the porous sol-gel derived coatings, indicate that the addition of SF_6 had no effect upon the damage resistance of a porous coating. The difference in results can be attributed to the different approaches in performing the experiment.

Eron'ko, et. al., used a 1.06 μm laser with a 70 nsec pulse duration and a 60 μm spot size. They used multiple laser shots per test site, and the appearance of a plasma was taken as the criteria of damage occurring to a test site. A probability of the plasma occurring was then calculated by taking the ratio of the number of laser shots required for a plasma to occur to the total number of laser shots taken per test site (~4000 shots). These probabilities were then used as an indication of damage resistance.

For this thesis, a 1.06 μm laser with a 5 nsec pulse duration and a 148 μm spot size was used. Each test site was subjected to only one laser shot and damage was determined by a visual inspection of the damage site. The damage threshold of each material was then calculated by equation (3).

As seen when comparing these two experiments, four basic differences arise: The difference in pulse duration, the spot size, the number of laser pulses per damage site, and the damage criteria.

The pulse duration has a direct effect upon the damaging process (Ref 37) in that the electric field strength required for damage is proportional to the pulse duration raised to the minus one fourth power, $t^{-1/4}$, and the energy density required for damage shows a $t^{-1/2}$ dependence. Thus, damaging an optical surface with a 5 nsec laser pulse would require

a higher energy density than damaging the material with a 70 nsec laser pulse. Thus, this pulse duration dependence would just change the values of the damage threshold of the material, and would not explain the contradictory results seen in the experiments.

In examining the spot size dependence upon laser-induced surface damage, one finds that smaller spot sizes (<100 μm) give a higher damage threshold for a material than the larger spot sizes (Ref 37). The reason for the higher thresholds with the smaller spot sizes is that the beam is less likely to encounter an imperfection in the material. Smaller spot sizes also tend to have larger spreads than the larger spots. Thus, the spot size dependence will just give different values for the damage threshold of a material, and again will not explain the contradictory experimental results.

Multiple laser pulses per test site has the effect of conditioning the test site and making it harder to damage (Ref 38), while with a single laser pulse per test site, there is either damage or no damage and no conditioning can occur. This conditioning due to multiple laser pulses occurs with the first few laser pulses which remove microimperfections in the material, improving the surface and making it harder to damage. Eron'ko, et. al., used multiple laser pulses per test site, but they also observed that there was still an increase in the damage threshold with the addition of SF_6 from the first flash, or for the first laser pulse, i.e., a single laser pulse testing. Thus, the conditioning effect due to multiple laser pulses also does not explain the contradicting experimental results.

The last difference between the two experiments is the damage criteria. Eron'ko, et. al., used a visible plasma as an indicator for damage, while

this thesis made a visible inspection of each test site for damage to the material. A visible plasma generally indicates that major damage has occurred to the material, but minor damage can also occur to the surface without a visible plasma being present. This minor damage is generally small pits formed by the absorbing impurities in the material. However, the formation of the visible plasma is through an electron avalanche process, which can be affected by the presence of an electronegative gas. Thus, the contradictory experimental results can be explained since a visible plasma will be more difficult to achieve in the presence of an electronegative gas, yielding an increase in damage resistance, according to Eron'ko; while the small pits and minor damage which occur from absorbing impurities is unaffected by the presence of an electronegative gas. Thus, the visible inspection of each test site located the presence of any type of damage, small pits to major damage, while using a visible plasma as an indicator of damage did not include these initial damage sites, which explains the difference in the experimental results.

Recommendations For Future Research

This experiment examined the effects of electronegative gases upon the damage threshold of a material, however, this study concentrated only on single laser pulse testing of the material. Further study is needed for multiple laser shots per test site, or N-on-1 testing, in order to measure conditioning effects and to obtain survivability curves.

The porous surface samples used in this study had slightly nonhomogeneous surfaces which often caused unusually large spreads. Further research with porous surfaces should be made with samples which have more homogeneous surfaces so as to reduce the spreads and to give a more accurate value for the damage threshold.

The effect of electronegative gases upon the electron density growth rate should also be investigated. The growth rate of the electron number density could be measured with a proportional counter to determine whether the presence of an electronegative gas will hinder the electron density growth rate and the formation of a plasma.

Bibliography

1. Damage in Laser Glass, ASTM Special Technical Publication 469, eds. A. J. Glass and A. H. Guenther, (1969).

2. Damage in Laser Materials, NBS Special Publication 341, eds. A. J. Glass and A. H. Guenther, US GPO Washington DC, (1970).

3. Damage in Laser Materials: 1971, NBS Special Publication 356, eds. A. J. Glass and A. H. Guenther, US GPO Washington DC, (1971).

4. Laser-Induced Damage in Optical Materials: 1972, NBS Special Publication 372, eds. A. J. Glass and A. H. Guenther, US GPO Washington DC, (1972).

5. Laser-Induced Damage in Optical Materials: 1973, NBS Special Publication 387, eds. A. J. Glass and A. H. Guenther, US GPO Washington DC, (1973).

6. Laser-Induced Damage in Optical Materials: 1974, NBS Special Publication 414, eds. A. J. Glass and A. H. Guenther, US GPO Washington DC, (1974).

7. Laser-Induced Damage in Optical Materials: 1975, NBS Special Publication 435, eds. A. J. Glass and A. H. Guenther, US GPO Washington DC, (1975).

8. Laser-Induced Damage in Optical Materials: 1976, NBS Special Publication 462, eds. A. J. Glass and A. H. Guenther, US GPO Washington DC, (1976).

9. Laser-Induced Damage in Optical Materials: 1977, NBS Special Publication 509, eds. A. J. Glass and A. H. Guenther, US GPO Washington DC, (1977).

10. Laser-Induced Damage in Optical Materials: 1978, NBS Special Publication 541, eds. A. J. Glass and A. H. Guenther, US GPO Washington DC, (1978).

11. Laser-Induced Damage in Optical Materials: 1979, NBS Special Publication 568, eds. H. Bennett, A.J. Glass, A. H. Guenther and B. E. Newman, US GPO Washington DC, (1979).

12. Laser-Induced Damage in Optical Materials: 1980, NBS Special Publication 620, eds. H. Bennett, A.J. Glass, A. H. Guenther and B. E. Newman, US GPO Washington DC, (1980).

13. Yamanaka, C., et. al. "Investigation of Damage in Laser Glass," Damage in Laser Materials: 1971, NBS Special Publication 356, eds. A. J. Glass and A. H. Guenther, US GPO Washington DC, (1971).

14. Artem'ev, V. A., et. al. "Chemical Reactions in the Presence of Optical Breakdown of Dielectric Coatings," Izvestiya Akademii Nauk SSSR, Seriya Fizicheskaya, Vol. 44, No. 10, pp. 2108-12, (1980).

15. Sparks, M. "Current Status of Electron-Avalanche Breakdown Theories," Laser-Induced Damage in Optical Materials: 1975, NBS Special Publication 435, eds. A. J. Glass and A. H. Guenther, US GPO Washington DC, (1975).

16. Vaidyanathan, A., et. al. "Competing Mechanisms in Laser-Induced Damage," Laser-Induced Damage in Optical Materials: 1979, NBS Special Publication 568, eds. H. Bennett, A.J. Glass, A. H. Guenther and B. E. Newman, US GPO Washington DC, (1979).

17. Sparks, M., et. al. "Theory of Electron-Avalanche Breakdown in Solids," Laser-Induced Damage in Optical Materials: 1979, NBS Special Publication 568, eds. H. Bennett, A.J. Glass, A. H. Guenther and B. E. Newman, US GPO Washington DC, (1979).

18. Walker, T. W., et. al. "Pulsed Laser-Induced Damage to Thin-Film Optical Coatings - Part I: Experimental," IEEE Journal of Quantum Electronics, Vol. QE-17, No. 10, pp. 2041-52, (Oct. 1981).

19. Sharma, B. S. and Klaus E. Rieckhoff, "Laser-Induced Dielectric Breakdown and Mechanical Damage in Silicate Glasses," Canadian Journal of Physics, Vol 48, pp. 1178-91, (1970).

20. Wright, J. K. "Theory of Electrical Breakdown of Glasses by Intense Pulses of Light," Proc. Phys. Soc., Vol 84, pp. 41-6, (1964).

21. Gagarin, A. P., et. al. "Dynamics of Surface Optical Breakdown in Glass," Sov. Tech. Phys. Lett. 3(9), pp. 392-95, (Sept. 1977).

22. Denileiko, Yu K., et. al. "Role of Absorbing Defects in the Mechanism of Laser Damage of Real Transparent Dielectrics," Sov. J. Quan. Electron., Vol 4, No. 8, pp. 1005-8, (Feb. 1975).

23. Aleshin, I. V., et. al. "Optical Breakdown of Transparent Media Containing Microinhomogeneities," Sov. Phys. JETP, Vol 43, No. 4, pp. 631-36, (April 1976).

24. Eron'ko, S. B., et. al. "On Increasing the Resistance of Glass Surfaces to Repeated Radiation Loads," Sov. J. Opt. Technol., Vol 43, No. 1, pp. 29-31, (Jan. 1976).

25. Fehsenfeld, F. C. "Electron Attachment to SF_6," Journal of Chemical Physics, Vol 53, No. 5, pp. 2000-4, (1 Sept. 1970).

26. Hickam, W. M. and R. E. Fox, "Electron Attachment in Sulfurhexaflouride using Monoenergetic Electrons," Journal of Chemical Physics, Vol 25, No. 4, pp. 642-7, (Oct. 1975).

27. Mason, J. P., et. al. "Arc Stability of Electronegative Gases," IEEE Transactions on Electrical Insulation, Vol EI-2, No. 1, pp. 1-10, (April 1967).

28. Walker, T. W., Laser-Induced Damage to Thin Film Dielectric Coatings, PhD Dissertation, Wright-Patterson AFB, Ohio: School of Engineering AFIT (April 1980).

29. HOYA's ARG-2, Technical Report, HOYA Optics USA, Inc., (1 Feb. 1980).

30. Brinker, C. J. and Mukherjee, S. P., "Conversion of Monolithic Gels to Glasses in a Multicomponent Silicate Glass System," Thin Solid Films, 77, pp. 141-8, (1981)

31. Pettit, R. B. and Brinker, C. J., "Sol-Gel Protective Coatings for Black Chrome Solar Selection Films," SPIE Vol 325, Optical Coatings for Energy Efficiency and Solar Application, pp. 1980-88, (1982).

32. Milan, D., "Damage Resistant Antireflection Surfaces for High Power Lasers," Defense Programs, pp. 9-17, (1982).

33. Brinker, C. J. and Harrington, Mark, Sandia National Laboratories, Albuquerque, New Mexico, Private Communication.

34. Newman, B. E., et. al. "Influence of Standing-Wave Fields on the Damage Resistance of Dielectric Films," Laser-Induced Damage in Optical Materials: 1975, NBS Special Publication 435, eds. A. J. Glass and A. H. Guenther, US GPO Washington DC, (1975).

35. Bettis, J. R., "Laser-Induced Damage as a function of Dielectric Properties at 1.06 μm." PhD Dissertation, Wright-Patterson AFB, Ohio: School of Engineering AFIT, (March 1975).

36. House, R. A. II, "The Effects of Surface Structure Properties on Laser-Induced Damage at 1.06 μm," PhD Dissertation, Wright-Patterson AFB, Ohio: School of Engineering AFIT (March 1975).

37. Bettis, J. R., et. al. "Spot Size and Pulse Duration Dependence of Laser-Induced Damage," Laser-Induced Damage in Optical Materials: 1976, NBS Special Publication 462, A. J. Glass and A. H. Guenther, US GPO Washington DC (1976).

38. Tikhomirov, G. P., and Turovskaya, T. S., "Electron-Microscope Studies of the Pre-Threshold Changes in Optical Glass Arising from the Action of Laser Radiation," Opt. Mekh. Promst. 44, pp. 65-67, (May 1977).

Vita

John A. Kardach was born on August 15, 1959, in Memphis, Tennessee. He obtained his undergraduate degree in Physics at Angelo State University, San Angelo, Texas, in May of 1981. After obtaining his commission in the U.S. Air Force in May of 1981, he proceeded to Wright-Patterson AFB, Ohio, where he is presently studying for a Master's Degree in Physics at the Air Force Institute of Technology.

UNCLASSIFIED

SECURITY CLASSIFICATION OF THIS PAGE *(When Data Entered)*

REPORT DOCUMENTATION PAGE		READ INSTRUCTIONS BEFORE COMPLETING FORM
1. REPORT NUMBER AFIT/GEP/PH/82D-16	2. GOVT ACCESSION NO. AD-A124 718	3. RECIPIENT'S CATALOG NUMBER
4. TITLE *(and Subtitle)* DEPENDENCE OF PULSED LASER-INDUCED DAMAGE TO OPTICAL SURFACES ON THE SPECIES AND PRESSURE OF AN AMBIENT GAS		5. TYPE OF REPORT & PERIOD COVERED MS Thesis 6. PERFORMING ORG. REPORT NUMBER
7. AUTHOR(s) John A. Kardach 2nd Lt. USAF		8. CONTRACT OR GRANT NUMBER(s)
9. PERFORMING ORGANIZATION NAME AND ADDRESS Air Force Institute of Technology (AFIT-EN) Wright-Patterson AFB, OH 43433		10. PROGRAM ELEMENT, PROJECT, TASK AREA & WORK UNIT NUMBERS 61101F
11. CONTROLLING OFFICE NAME AND ADDRESS Air Force Weapons Laboratory (AFWL) Kirtland AFB, NM 87117		12. REPORT DATE December 1982 13. NUMBER OF PAGES 52
14. MONITORING AGENCY NAME & ADDRESS*(if different from Controlling Office)*		15. SECURITY CLASS. *(of this report)* UNCLASSIFIED 15a. DECLASSIFICATION/DOWNGRADING SCHEDULE

16. DISTRIBUTION STATEMENT *(of this Report)*

Approved For Public Release; Distribution Unlimited

17. DISTRIBUTION STATEMENT *(of the abstract entered in Block 20, if different from Report)*

18. SUPPLEMENTARY NOTES

Approved for public release: IAW AFR 190-17.

LYNN E. WOLAVER
Dean for Research and Professional Development
Air Force Institute of Technology (AFIT)
Wright-Patterson AFB OH 45433

6 JAN 1983

19. KEY WORDS *(Continue on reverse side if necessary and identify by block number)*

Laser Damage
Electronegative Gases

20. ABSTRACT *(Continue on reverse side if necessary and identify by block number)*

The testing of optical materials in electronegative gases was investigated to determine if an increase in the resistance of the material to pulsed laser-induced damage could be realized as indicated by the Soviet literature. The materials were irradiated with a 1.06 μm laser pulse of 5 nsec and a spot size ($1/e^2$ radius) of 148 μm. The materials used for testing consisted of ~~ZnO~~, dielectric thin films (λ/2 at 1.06 μm), copper mirrors, fused silica substrates, Hoya's ARG-2 Glass, and porous sol-gel derived coatings. Each material was tested in environments of N_2, CF_4, and SF_6 for pressures

Nitrogen, Tetrafluoromethane, Sulfur hexafluoride

DD FORM 1 JAN 73 1473 EDITION OF 1 NOV 65 IS OBSOLETE

SECURITY CLASSIFICATION OF THIS PAGE *(When Data Entered)*

ranging from less than 10^{-5} torr to 600 torr. The results indicated that the energy density damage threshold was unaffected by the type or pressure of the gas surrounding the material for single shot damage testing.

* Eron'ko, S.B., G.T. Petrovskii, A.V. Shatilov, A.K. Yakhkind, and L.V. Alcksandrova, "On Increasing the Resistance of Glass Surfaces to Repeated Radiation Loads," Sov. J. Opt. Technol., Vol 43, No. 1, pp. 29-31 (Jan 1976).